Structural Engineering and Mechanics, *Vol. 71, No. 3 (2019) 291-303*
DOI: https://doi.org/10.12989/sem.2019.71.3.291

Spectral element method in the analysis of vibrations of overhead transmission line in damping environment

Maciej Dutkiewicz[1*] and Marcela Machado[2]

[1]*Faculty of Civil, Environmental Engineering and Architecture, University of Science and Technology, 85-796 Bydgoszcz, Poland*
[2]*Department of Mechanical Engineering, University of Brasilia, 70910-900, Brasilia, Brazil*

(Received January 18, 2019, Revised March 15, 2019, Accepted April 3, 2019)

Abstract. In the paper the analysis of natural vibrations of the transmission line with use of spectral elements and the laboratory experiments is performed. The purpose of the investigation is to analyze the natural vibrations of the transmission line and compare with the results obtained in the numerical simulations. Particular attention is paid to the hysteretic and aerodynamic damping analysis. Sensitivity of the wave number is performed for changing of the tension force, as well as for the different damping parameters. The numerical model is made using the Spectral Element Method. In the spectral model, for various parameters of stiffness, damping and tension force, the system response is checked and compared with the results of the accelerations obtained in the measurements. A frequency response functions (FRF) are calculated. The credibility of the model is assessed through a validation process carried out by comparing graphical plots of FRF and time history analysis and numerical values expressing differences in acceleration amplitude (MSG), phase angle differences (PSG) and differences in acceleration and phase angle total (CSG) values. The next aspect constituting the purpose of this paper is to present the wide possibilities of modelling and simulation of slender conductors using the Spectral Element Method. The obtained results show good accuracy in the range of both experimental measurements as well as simulation analysis. The paper emphasizes the ease with which the sensitivity of the conductor and its response to changes in density of spectral mesh division, tensile strength or material damping can be studied.

Keywords: spectral element method; hysteretic and aerodynamic damping; power transmission lines; validation metrix

1. Introduction

The rapid development of technology causes that modern construction objects have high strength parameters with low structural stiffness and low damping coefficient. These objects are particularly susceptible to dynamic load such as wind. Such structures include among others: tall buildings, chimneys, masts, suspended and cable stayed bridges and overhead transmission lines.

Transmission lines are constantly subjected to variable wind loads which may gradually lead to the impairment of their durability, resulting in the shortened service life. That is the huge need to design and construct the transmission lines with the respect of wide range of load cases acting on these slender structures. This is very important to develop the easy and fast methodology for design, taking into consideration all loads and uncertainities. Nowadays we see the wide development of new materials and solutions to increase the conductivity but at the same time we observe that conductors' durability is change and require the permanent update analysis. Spectral element method seems to be such fast and easy tool which fulfills these requirements.

There are some theoretical and experimental researches on transmission lines (Wang *et al*. 1997, Vecchiarelli *et al* 2000, Meynen 2005, Gołębiowska *et al*. 2015, Dutkiewicz 2017a). Wind forces cause three main types of conductor vibrations: aeolian vibrations with a frequency from 3 to 150 Hz and amplitudes lower than the conductor diameter, galloping with a frequency from 0.1 to 1 Hz and amplitudes from ±0.1 to 1 of conductor sag, wake induced vibrations with a frequency from 0.15 to 10 Hz and amplitudes from 0.5 to 80 times the conductor diameter (Gołębiowska and Dutkiewicz 2016, 2017a,b, Dutkiewicz 2017b).

The majority of common wind induced vibrations are aeolian vibrations. These vibrations are generated as a result of vortices shed in the conductor wake under sustained wind of low speed from 1 to 7 m/s – they occur mainly in the vertical plane (Dutkiewicz 2017b), Vibrations of conductors, both single and in a bundle, form standing waves with forced nodes and intermediate nodes located along the span at intervals depending on the frequency of free vibrations. When the conductor wind flow is laminar, alternately shedding vortices are formed in two points of the suction zone and make the conductor move perpendicularly towards the wind direction. The alternate shedding of vortices is regular. As a result, a so-called Karman vortex street is formed. When the frequency of the shedding of vortices is approximately equal to one of the frequencies of free vibrations of a conductor, a 'lock-in' phenomenon occurs. During this frequency synchronisation, the conductor is in the resonance state. Aeolian vibrations occur on single conductors and conductors in a bundle. Although these vibrations are hardly noticeable due to low amplitude values (lower than the conductor diameter), they are very

∗Corresponding author, Ph.D.
E-mail: macdut@utp.edu.pl

http://www.techno-press.com/journals/sem&subpage=7
ISSN: 1225-4568 (Print), 1598-6217 (Online)

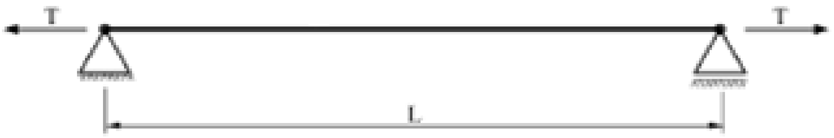

Fig. 1 Analysed model

important, since they can lead to fatigue destruction of a conductor in points of high stress concentrations.

Galloping is an aeroelastic self-excitation phenomenon characterised by low frequencies and high amplitudes, and it refers to single conductors and conductors in a bundle, with one or two loops of standing and running waves, or their combination in a conductor span. Standing waves may have one or more loops (up to 10) over the span length. However, a small number of loops is predominant. In most cases, galloping is caused by sustained wind of an average and high speed (V > 15 m/s), blowing on an asymmetrically loaded (e.g. with ice or wet snow) conductor. High amplitudes are observed in the vertical plane, whereas the frequencies depend on the type of a conductor and vibrations (Gołębiowska *et al*. 2015). Galloping is a typical instability caused by the coupling of aerodynamic forces which affect the conductor with its vibrations. Conductor vibrations change the wind angle of attack on a periodic basis. The change of the angle of attack results in a change of aerodynamic forces affecting the conductor, which consequently changes the conductor response. The first, simplified criterion (if a single degree-of-freedom system is applied) pertaining to the instability connected with galloping was presented by Den Hartog (1932) and developed by other researchers (Gołębiowska and Dutkiewicz 2018). A precondition for galloping (on the basis of the quasi-steady theory) is the presence of negative aeroelastic damping in the system. A conductor of a circular section cannot gallop due to its geometrical symmetry (dCL/dα=0), unless this section is changed. Icing of a conductor changes its cross-section, thus it leads to its aerodynamic instability. Research works carried out by Den Hartog indicate that the aerodynamic instability is the main reason for the galloping phenomenon. His research was conducted with an assumption that the vertical motion of a conductor is predominant, and the effect of torsional and horizontal motions can be ignored. Further research proved that the torsional motion is an integral part of the galloping phenomenon. The effect of a coupled torsional-translational motion plays a crucial role in most cases of progressing galloping (Luongo *et al*. 2009).

These extremely important phenomena described above have mobilized the authors of the article to look for transmission line vibration solutions using numerical methods. Spectral Element Method (SEM) proved to be such a method. SEM is a meshing method similar to Finite Element Method (FEM), where the approximated element shape functions are substituted by exact dynamic shape functions obtained from the exact solution of governing differential equations. Therefore, a single element is sufficient to model any continuous and uniform part of the structure. This feature reduces significantly the number of elements required in the structure model and improves the accuracy of the dynamic system solution. At the same time, there are some drawbacks like the unavailability of exact wave solutions for most complex and 2D and 3D structures. In these cases, approximated spectral element modelling can be used and may still provide very accurate solutions. In recent years some researchers were performed with use of SEM. The extensive study of the fundamentals and a variety of new applications such as composite laminated, periodic lattice, damage detection was presented in (Lee 2004). The wave behaviour in composites and inhomogeneous media is studied in (Gopalakrishnan et. al 2007). Studies related to structural damage detection have been developed in (Fabro *et al*. 2010). Other works using wave propagation and SEM to detect damage under the presence of structural randomness can also be found in references (Flynn *et al*. 2011, Machado and Santos 2015, Machado *et al*. 2017). The spectral element method for the vibration analysis of a multi-span beam subjected to a moving point force was analysed by Boseop *et al*. (2018). An enhanced spectral element model was proposed by Lee *et al* (2017) for a functionally graded material (FGM) bar model in which axial and radial displacements in the radial direction are treated by representing the inner FGM layer by multiple sub-layers.

2. Mathematical model of transmission line

2.1 Beam spectral element subjected to a tensile load with structural damping

Considering a simplified cable model, as shown in Fig.1, the governing differential equation for the undamped free vibration is given by Clough and Penzien (1993) and Yu and Soliman (2014):

$$EI\frac{\partial^4 v}{\partial x^4} - T\frac{\partial^2 v}{\partial x^2} + \rho A\frac{\partial^2 v(x,t)}{\partial t^2} = 0 \qquad (1)$$

For a simply supported beam under axial force the natural frequency can be written as (Rao 2008):

$$\omega_n = \frac{\pi^2}{L^2}\sqrt{\frac{EI}{\rho A}}\left(n^4 + \frac{n^2 T L^2}{\pi^2 EI}\right)^{\frac{1}{2}}, \quad n = 1,2,\ldots \qquad (2)$$

where ρA is mass per unit length, EI the uniform bending rigidity, L is cable length, T is tension force, and $v(x,t)$ is the cable displacement as a function of the position x and time t.

The undamped Euler-Bernoulli beam equation of motion subjected to axial force and under bending vibration is governed by Eq. (1). Fig. 2 shows an elastic two-node

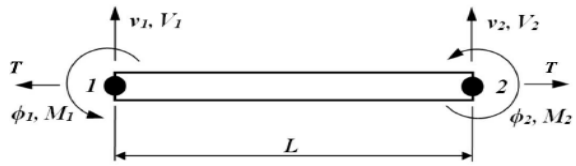

Fig. 2 Two-node spectral element

element with a uniform rectangular cross-section subjected to an axial force, where the properties are assumed to be deterministic variables. A structural internal damping is introduced into the beam formulation by adding into Young´s modulus weighted by a complex damping factor $i\eta, i = \sqrt{-1}, \eta$ is the hysteretic structural loss factor, to obtain $E = E(1 + i\eta)$.

By considering a constant coefficient a displacement solution can be assumed of the form (Dutkiewicz and Machado 2019 a,b):

$$v(x,t) = v_0 e^{-i(kx-\omega t)} \tag{3}$$

where v_0 is a amplitude, ω is the frequency and k is the wave number. Substituting it into Eq. (1), the dispersion equation is given by:

$$k^4 EI + k^2 T - \omega^2 \rho A = 0 \tag{4}$$

There are two distinct wave modes in the positive direction (k^2), which is positive-going waves with wave numbers given as:

$$k_1 = \sqrt{-\frac{T}{2EI} + \sqrt{\left(\frac{T}{2EI}\right)^2 + \frac{\rho A \omega^2}{EI}}} \tag{5}$$

$$k_2 = -\sqrt{-\frac{T}{2EI} - \sqrt{\left(\frac{T}{2EI}\right)^2 + \frac{\rho A \omega^2}{EI}}} \tag{6}$$

The general solution for the Euler-Bernoulli beam spectral element subjected to axial load of length L, can be expressed in the form:

$$\begin{aligned} v(x,\omega) = a_1 e^{-ikx} + a_2 e^{-kx} + a_3 e^{-ik(L-x)} \\ + \quad + a_4 e^{-k(L-x)} = \boldsymbol{s}(x,\omega)\boldsymbol{a} \end{aligned} \tag{7}$$

where

$$\boldsymbol{s}(x,\omega) = \{e^{-ikx}, e^{-kx}, e^{-ik(L-x)}, e^{-k(L-x)}\} \tag{8}$$

$$\boldsymbol{a}(x,\omega) = \{a_1, a_2, a_3, a_4\}^T \tag{9}$$

The spectral nodal displacements and slopes of the beam element are related to the displacement field at node 1 (x=0) and node 2 (x=L), by

$$\mathbf{d} = \begin{bmatrix} v_1 \\ \phi_2 \\ v_2 \\ \phi_2 \end{bmatrix} = \begin{bmatrix} v(0) \\ v'(0) \\ v(L) \\ v'(L) \end{bmatrix} \tag{10}$$

By substituting Eq. (7) into the right-hand side of Eq. (10) and written in a matrix form gives

$$\mathbf{d} = \begin{bmatrix} s(0,\omega) \\ s'(0,\omega) \\ s(L,\omega) \\ s'(L,\omega) \end{bmatrix} \boldsymbol{a} = \boldsymbol{G}(\omega)\boldsymbol{a} \tag{11}$$

where

$$\boldsymbol{G}(\omega) = \mathbf{d} = \begin{bmatrix} 1 & 1 & e^{-ikL} & e^{-kL} \\ -ik & -k & ike^{-ikL} & ke^{-kL} \\ e^{-ikL} & e^{-kL} & 1 & 1 \\ -ike^{-ikL} & -ke^{-kL} & ik & k \end{bmatrix} \tag{12}$$

The frequency-dependent displacement within an element is interpolated from the nodal displacement vector $\boldsymbol{d}$, by eliminating the constant vector $\boldsymbol{a}$ from Eq. (7) and using Eq. (11) it is expressed as:

$$v(x,\omega) = \boldsymbol{g}(x,\omega)\boldsymbol{d} \tag{13}$$

where the shape function is

$$\boldsymbol{g}(\boldsymbol{x},\omega) = \boldsymbol{s}(\boldsymbol{x},\omega)\boldsymbol{G}^{-1}(\omega) = \boldsymbol{s}(\boldsymbol{x},\omega)\boldsymbol{\Gamma}(\omega) \tag{14}$$

The dynamic stiffness matrix for the spectral beam element under axial tension can be determined as

$$\boldsymbol{S}(\omega) = \boldsymbol{K}(\omega) - \omega^2 \boldsymbol{M}(\omega) \tag{15}$$

where

$$\boldsymbol{K}(\omega) = \int_0^L \left(EI\boldsymbol{g}''(x)^T \boldsymbol{g}''(x) + T\boldsymbol{g}'(x)^T \boldsymbol{g}'(x)\right) dx \tag{16}$$

$$\boldsymbol{M}(\omega) = \rho A \int_0^L \boldsymbol{g}(x)^T \boldsymbol{g}(\boldsymbol{x}) \boldsymbol{dx} \tag{17}$$

where the prime (') denotes the derivative with respective to the spatial coordinate x. By solving the integral, the dynamic stiffness matrix is

$$\boldsymbol{S}(\omega) = \frac{\mathrm{EI}}{\Delta} \begin{bmatrix} s_{11} & s_{12} s_{13} s_{14} \\ & s_{22} s_{23} s_{24} \\ & s_{33} s_{34} \\ sym & s_{44} \end{bmatrix} \tag{18}$$

where $\Delta = \cos(k\,L)\cosh(k\,L) - 1$ and the components of element matrix (Eq.18) are given as

$$\begin{aligned} s_{11} &= -k^3(cos(kL)sinh\,(kL) + sin(kL)cosh(kL)) \\ s_{12} &= -k^2 sin\,(kL)sinh\,(kL) \\ s_{13} &= k^3\,(sin\,(kL) + sinh\,(kL)) \\ s_{14} &= k^2\,(cos(kL) - cosh(kL)) \\ s_{22} &= k(cos(kL)sinh(kL) - sin(kL)\,cosh(kL)) \\ s_{23} &= k^2(cosh(kL) - cos(kL)) \\ s_{24} &= k(sin\,(kL) - sinh(kL)) \\ s_{33} &= -k^3(cos(kL)sinh(kL) + sin(kL)cosh(kL)) \\ s_{34} &= k^2\,sin(kL)\,sinh(kL) \\ s_{44} &= k(cos(kL)\,sinh(kL) - sin(kL)\,cosh(kL)) \end{aligned} \tag{19}$$

2.2 Beam spectral element subjected to a tensile load with aerodynamic and friction damping

As far as structure beam is uniform without any sources of discontinuity, it can be represented by a single spectral element with very accurate solutions (Doyle 1997). However, if there exist sources of discontinuity such as the point loads the beam should be spatially discretized into spectral elements. Analogous to Finite Element Method (FEM) (Zienkiewicz 1991), the spectral elements can be assembled to form a global structure matrix system (Lee 2009). As presented in last section the cable was modelled as an equivalent homogeneous Euler-Bernoulli beam with constant bending stiffness, subjected to a constant tensile load, and assuming hysteretic damping. However, it is known that overhead conductors works exposed to wind gust, random winds and different weather conditions. Such environment can influence the cable vibration. The simple cable dynamic model as presented in Eq.1 have been frequently applied in the literature. Concerning with the aerodynamic damping, which can be associated with the energy dissipation due to friction between the vibrating conductor and surrounding air, and the conductor self-damping represented by a linear damping model derived from the Kelvin-Voigt constitutive relationship where the friction among the conductor wires is related to the curvature during bending vibrations, the following governing equation is proposed (Matt and Castello 2007)

$$EI\frac{\partial^4 v}{\partial x^4} - T\frac{\partial^2 v}{\partial x^2} + \xi I\frac{\partial}{\partial t}\left(\frac{\partial^4 v}{\partial x^4}\right) + \alpha\frac{\partial v(x,t)}{\partial t} + \rho A\frac{\partial^2 v(x,t)}{\partial t^2} = 0 \tag{20}$$

where ρA is mass per unit length, α stands for a viscous-like aerodynamic damping, E is the Young modulus and ξI represents the energy dissipation mechanism associated with the inter-strand friction among the wires of a typical conductor, ξ is material damping factor. The equilibrium equation (20) at frequency domain can be written as:

$$EI\frac{\partial^4 v}{\partial x^4} - T\frac{\partial^2 v}{\partial x^2} + \xi I\frac{\partial}{\partial t}\left(\frac{\partial^4 v}{\partial x^4}\right) + (i\omega\alpha + \omega^2\rho A)v = 0 \tag{21}$$

In this work, beside the dynamic behaviour of the conductor we are also interested from the wave propagation perspective. By considering a constant coefficient, a displacement solution can be assumed in the form of Eq. (3). Substituting $v(x,t)$ into Eq. (20), the dispersion equation is given by:

$$k^4EI - k^2T + \omega k^4\xi I + \omega\alpha - \omega^2\rho A = 0 \tag{22}$$

By solving the Eq. (22) in function of the quadratic term of k^2, there are two distinct wave modes in the positive direction with wave numbers expressed as:

$$k_1 = \sqrt{-\frac{T}{2EI + 2\xi I} + \sqrt{\left(\frac{T}{2EI + 2\xi I}\right)^2 + \frac{\alpha\omega + \rho A\omega^2}{EI + \xi I}}} \tag{23}$$

$$k_2 = \sqrt{-\frac{T}{2EI + 2\xi I} - \sqrt{\left(\frac{T}{2EI + 2\xi I}\right)^2 + \frac{\alpha\omega + \rho A\omega^2}{EI + \xi I}}} \tag{24}$$

The other two distinct wave modes in the negative direction, i.e. negative-going waves, having wave numbers given by $k_3 = -k_1$ and $k_2 = -k_4$. The general solution for the Euler-Bernoulli beam spectral element subjected to axial load and shape function formulation are a similar procedure presented in Eqs. (7 - 13), where the shape function has the form of Eq.14.

The global damped dynamic spectral matrix for a deterministic system can be described as

$$\boldsymbol{S}(\omega) = \boldsymbol{K}(\omega) + i\omega C(\omega) - \omega^2\boldsymbol{M}(\omega) \tag{25}$$

$\boldsymbol{K}(\omega)$, $\boldsymbol{M}(\omega)$ are described by Eqs. (16-17), respectively, and the damping matrix can be rewritten as

$$\boldsymbol{C}(\omega) = \int_0^L (\xi I\boldsymbol{g}''(x)^T\boldsymbol{g}''(x) + \alpha g(x)^T g(x))dx \tag{26}$$

or as function of the element mass and stiffness matrices as follows:

$$\boldsymbol{C}(\omega) = \frac{\alpha}{\varrho A}M(\omega) + \int_0^L \left(\xi I\boldsymbol{g}''(x)^T\boldsymbol{g}''(x) + \alpha g(x)^T g(x)\right)dx = \frac{\alpha}{\varrho A}M(\omega) + \frac{\xi}{E}K(\omega) - \frac{\xi T}{E}\int_0^L g'(x)^T g'(x)dx \tag{27}$$

where the prime (') denotes the derivative with respective to the spatial coordinate x.

3. Validation and verification

The article presents a validation analysis in relation to the experimental and the simulation model. The essence of using computer simulation methods requires determining their level of accuracy in relation to direct measurement of the actual model. The required level of accuracy of the simulation depends on the purposes for which the simulation is applied. According to AIAA (1998) and ASME (2006) validation and verification are the basic tools used to determine the credibility of the used model. Validation explains how the model represents reality, while verification determines that the implementation of the model properly represents the adopted description and solutions of the model application. In the validation process, the accuracy is referred to the measurement results, in verification the accuracy is referred to the pattern obtained in the calculation model. Uncertainty and error are the reasons that affect the accuracy of results obtained in the modelling and simulation process. Uncertainty results from the lack of knowledge or incomplete knowledge about the physical characteristics, the analyzed parameter, wrong assumptions concerning, for example, the flow of wind around the analyzed body with different surface porosity, may result from the complexity of the phenomenon, eg wind turbulence. Errors can be classified as confirmed and unconfirmed (conscious and unconscious). Errors in rounding are confirmed errors, while programming errors are not anomalous errors. The validation strategy is to identify and quantify errors and uncertainties in the conceptual and computational model.

The strategy of model verification is connected with the identification and quantification of errors consisting in obtaining inappropriate convergence of spatial and temporal discretization, convergence of iterations and computer programming. The essence of verification consists in a detailed analysis of the size of the division grid and the time step. With the size of the grid size and the time step approaching zero, the discretization error should asymptotically reach zero.

Validation metrics is the subject of interest of many researchers. Oberkampf and Trucano (2002) present an extensive review of the literature in validation and verification (V&V) in computational fluid dynamics (CFD), discusses methods and procedures for assessing V&V, and develops a number of extensions to existing ideas. The review of the development of V&V terminology and methodology points out the contributions from members of the operations research, statistics, and CFD communities. Authors explain that the fundamental strategy of verification is the identification and quantification of errors in the computational model and its solution. A set of guidelines is proposed for designing and conducting validation experiments, supported by an explanation of how validation experiments are different from traditional experiments and testing. A description is given of a relatively new procedure for estimating experimental uncertainty that has proven more effective at estimating random and correlated bias errors in wind-tunnel experiments than traditional methods.

Aeschliman *et al*. (1995) describe a methodology for verification, calibration, and validation (VCV). A novel approach to uncertainty analysis is described which can both distinguish between and quantify various types of experimental error, and whose attributes are used to help define an appropriate experimental design for code VCV experiments.

Schwer (2007) presents developed metrics and their wave form comparative quantification was demonstrated through application to analytical wave forms, measured and computed free-field velocity histories, and comparison with Subject Matter Expert opinion.

William *et al*. (2014) propose a framework for assessing validation experiments for computational fluid dynamics regarding information content, data completeness, and uncertainty quantification. This framework combines two concepts: the concept of a strong-sense benchmark for validation experiments and the modelling assessment procedure referred to as the predictive capability maturity method. The validation experiment assessment requirements are captured in a table of attributes: Experimental Facility, Analog Instrumentation and Signal Processing, Boundary and Initial Conditions, Fluid and Material Properties, Test Conditions, and Measurement of System Responses and four levels of information completeness for each attribute.

William *et al*. (2006) develop a validation metric that is based on the statistical concept of confidence intervals. Using this fundamental concept, two specific metrics: one that requires interpolation of experimental data and one that requires regression (curve fitting) of experimental data. Authors discuss how the present metrics are easily interpretable for assessing computational model accuracy, as well as the impact of experimental measurement uncertainty on the accuracy assessment.

Russell (1997) develops a new set of magnitude, phase, and comprehensive error measures to evaluate the differences between two functions or test and analytical data. The error factors are on the same relative scale and have physical interpretations.

Geers (1984) presents the metric for comparing calculated transient response history with its measured counterpart. The proposed measure assigns a single numerical value to the discrepancy between the two histories over a specified comparison period. Computational of the measure involves the integration in time of squares and products of the calculated and measured histories. Representative results are shown for both idealized and actual response histories.

Validation metrics problems were developed also in works (Aeschliman and Oberkampf 1998, Barber 1998, Benek *et al*. 1998, Bertin *et al*. 1993, Bradley 1998, Coleman and Stern 1997, Mehta 1996, Sprague and Geers 2003).

In the present paper the formulation of the validation metrics is proposed as follows (Sprague and Geers 2003, Schwer 2007)

$$\vartheta_{mm} = (t_2 - t_1)^{-1} \int_{t_1}^{t_2} m^2\,(t)dt \tag{28}$$

$$\vartheta_{cc} = (t_2 - t_1)^{-1} \int_{t_1}^{t_2} c^2\,(t)dt \tag{29}$$

$$\vartheta_{mc} = (t_2 - t_1)^{-1} \int_{t_1}^{t_2} m\,(t)c(t)dt \tag{30}$$

where $m(t)$ is the measured history and $c(t)$ is the simulation history, $t_1 < t < t_2$ is the time span of interest for the response history. The amplitude validation metric (AVM) is:

$$M_{SG} = \sqrt{\frac{\vartheta_{cc}}{\vartheta_{mm}}} - 1 \tag{31}$$

The AVM is insensitive to phase discepancies and is based upon the area under the squared response history. The phase validation metric (PVM) is:

Table 1 Comparison of 10 firsts analytical natural frequency with resonance picks obtained in the simulations for different length L_l of spectral element, A=254.34mm^2, T=0.1 kN,η=0.01, simulation1 L_l=0.175m, simulation2 L_l=0.07m, simulation 3 L_l=0.035m

$\boldsymbol{\omega_n}$ **(Hz)**	3,98	12,65	26,89	46,78	72,34	103,58	140,49	183,08	231,35	285,30
Simulation 1	4	12,6	26,9	-	72,4	103,7	140,7	-	231,6	285,9
Simulation 2	4	12,6	26,9	46,8	72,3	103,6	140,8	183,3	232,9	-
Simulation 3	4	12,6	26,9	46,8	72,4	103,9	140,2	183,5	231,8	285,9

$$P = \frac{1}{\pi}\operatorname{acos}\left(\frac{\vartheta_{mc}}{\sqrt{\vartheta_{mm}\vartheta_{cc}}}\right) \tag{32}$$

PVM is insensitive to magnitude differences. The comprehensive validation metric is:

$$C_{SG} = \sqrt{{M_{SG}}^2 + P^2} \tag{33}$$

In the article, the validation process consisted in determining the validation coefficients and checking whether these coefficients are smaller than the assumed level of 30% in full range of analysed domain (Geers 1984). Checks were carried out for different stiffness and tension values within the fixed time range. During the analysis, also the damping factors were changed. In the work, the verification process was carried out for different grid densities – spectral element's length.

4. Numerical results

The first step of the analysis is to validate the proposed model. It is compared with the analytical solution and experimental tests. In both case, the conductor has simply supported ends with the same properties of the experimental tests, conductor with diameter of D = 18 mm, the weight per unit length of 0.656 kg/m, density of 2580 kg/m3, relative Young's modulos of 0.10 GPa, and the span length of L = 0.7 m. The aspect ratio of the conductor was about 38.89.

To compare the numerical model with analytical natural frequency solution described in the Eq. (2) it is required to estimate the natural frequencies from the FRF obtained through the SEM. Analysis was made for different length of the spectral element: L_l=[0.035, 0.07, 0.175]m. All 10 frequencies corresponding to the theoretical analysis were obtained for L_l = 0.035 (Table 1), for L_l = 0.07 the tenth natural frequency was omitted, for L_l = 0.175, the fourth and eight natural frequencies were omitted (Fig. 3)

The frequency response functions (FRF) and change of the dispersion curve (k) with tension force T=1000 kN and T=0.10 kN are showed in Fig. 4. For the higher tension force, T=1000 kN, the dispersion curve of the conductor presents a straight line generating a non-dispersive wave. The total natural frequencies were five for the range from 0 Hz to 1500 Hz. By decreasing of the tension force to T=0.10 kN the conductor changes the wave behaviour. The waves propagate dispersively and the number of natural frequency increased to twenty one in the frequency range from 0 Hz to 1500 Hz. Figs. 5 and 6 present the dispersion diagram for the conductor model with hysteretic and aerodynamic damping and different values of tension force. The wave numbers are calculated according to Eq. (5), for the tension force T = [0.1, 1, 10, 100, 1000, 10000] kN.

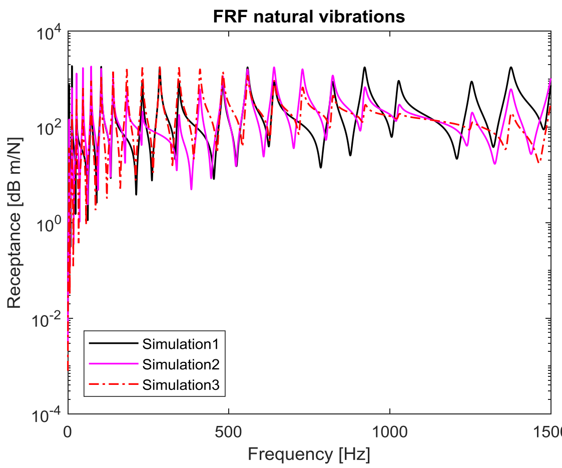

Fig. 3 Natural frequency identification for different length L_l of spectral element, A=254.34mm^2, T=0.1 kN,η=0.01, (a) simulation 1 L_l=0.175m, (b) simulation 2 L_l=0.07m, (c) simulation 3 L_l=0.035m

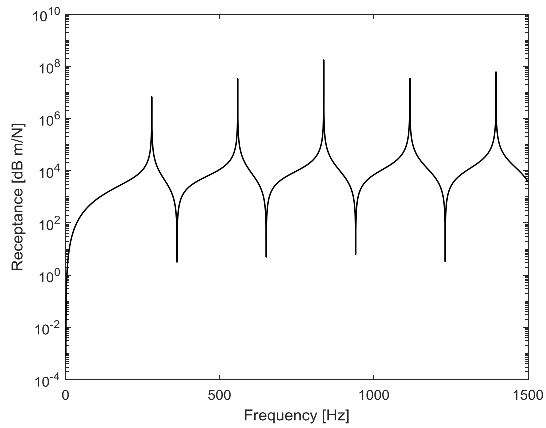

(a)

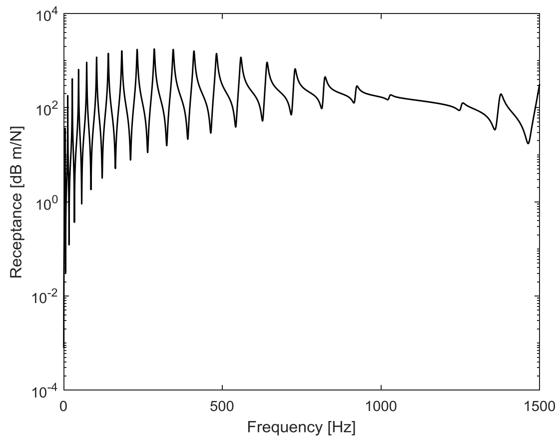

(b)

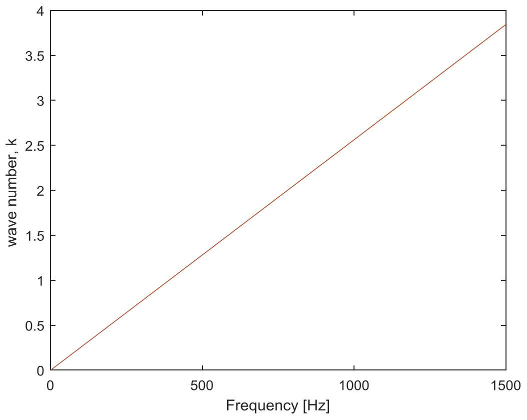

(c)

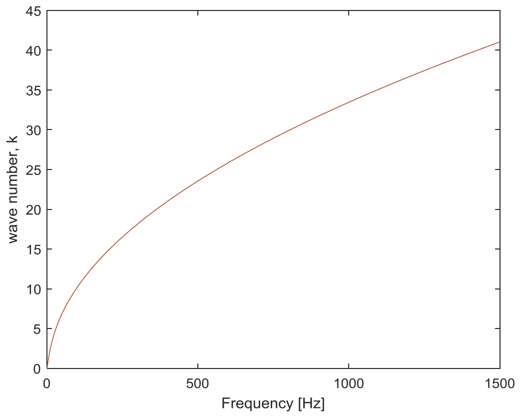

(d)

Fig. 4 FRFs and hysteretic dispersion curves, (a), (c) for tension force of T=1000 kN, (b), (d) for tension force of T=0.1kN

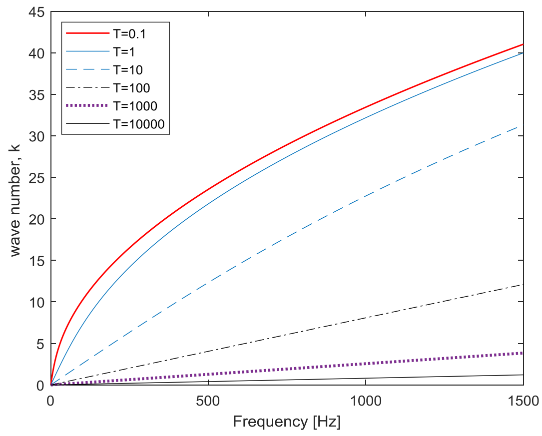

(a)

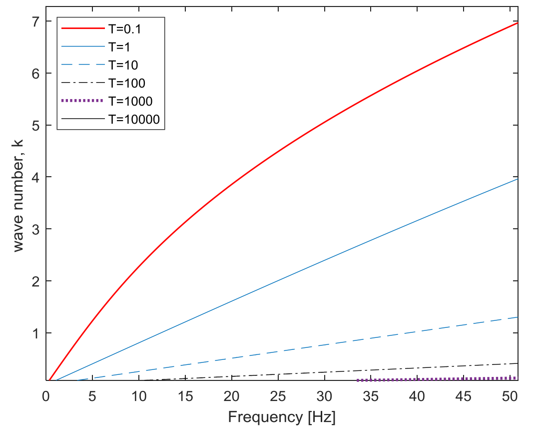

(b) Zoom

Fig. 5 Dispersion curves for hysteretic damping and different tension values, T = [0.1, 1, 10, 100, 1000, 10000] kN.

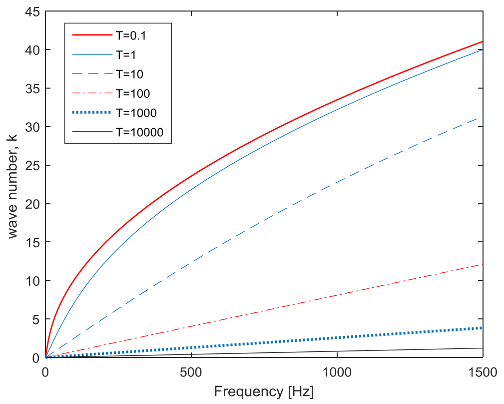

(a)

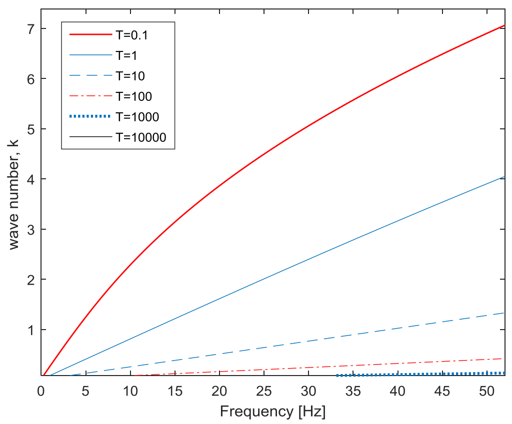

(b) Zoom

Fig. 6 Dispersion curves for aerodynamic damping and different tension values, T=[0.1, 1, 10, 100, 1000, 10000] kN.

The dispersion diagram of the conductor with a tension force of T = 0.10 kN, different material damping ratio ξ and aerodynamic damping α are shown in Figs. 7 and 8.

Figs. 9 (a) and (b) show the FRF functions for the natural vibration of the conductor for different value of aerodynamic damping α and fixed values of material damping ratio ξ. Figs. 9 (c) and (d) show the FRF functions for different value of material damping ratio ξ and fixed values of aerodynamic damping α, and Figs. 9 (e)and (f) for different value of hysteretic loss factor η.

The presented analysis shows the impact of the aerodynamic damping and hysteretic loss factor on frequency response functions. The change of aerodynamic damping causes the phase discepancies and hysteretic loss factor has the impact on values of amplitudes.

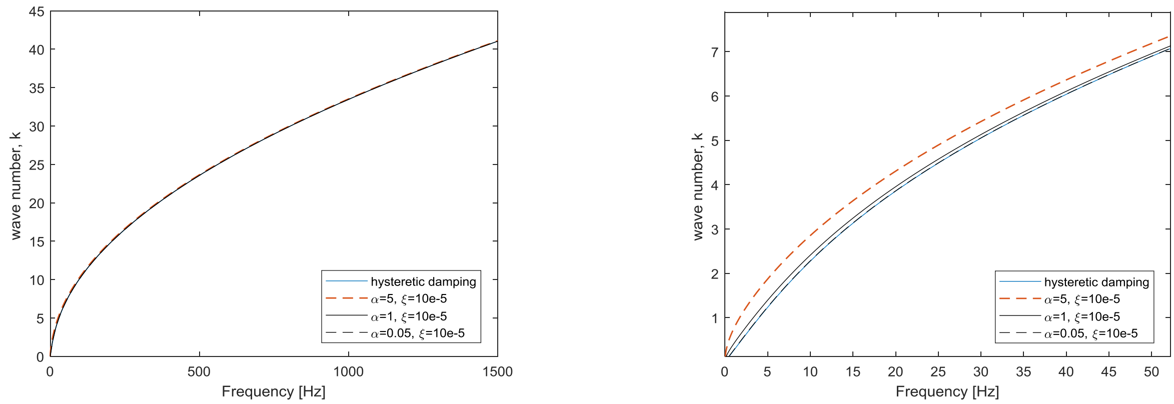

(a) (b) Zoom

Fig.7 Dispersion curves for tension force T=0.1 kN, different value of aerodynamic damping α and fixed material damping ratio ξ

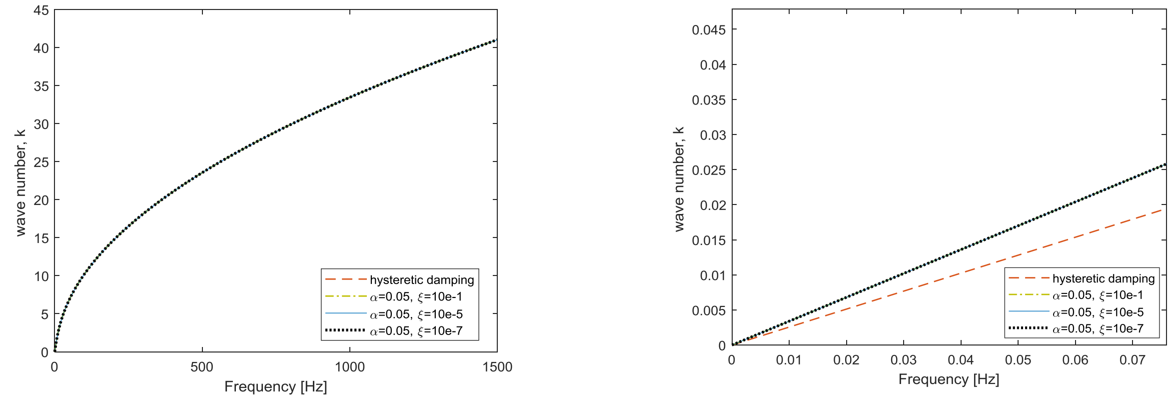

(a) (b) Zoom

Fig.8 Dispersion curves for tension force T=0.1 kN, different value of material damping ratio ξ and fixed aerodynamic damping α

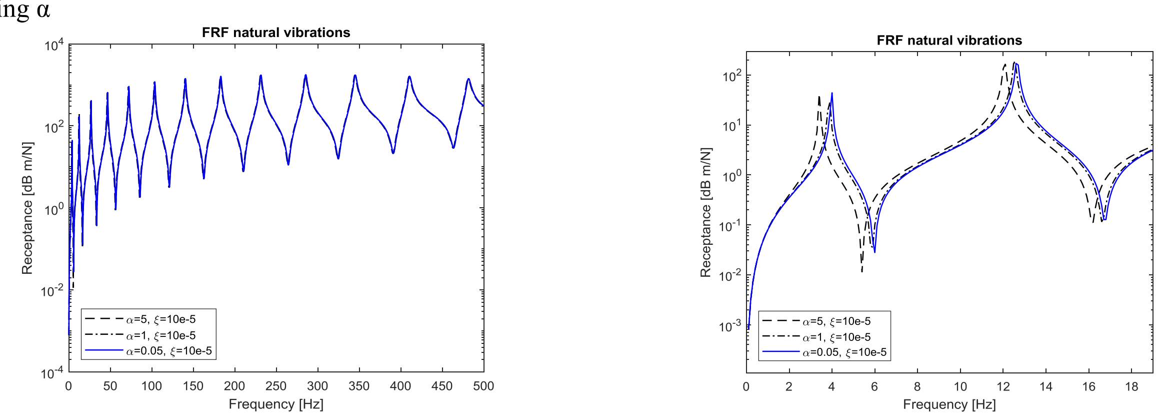

(a) (b) Zoom

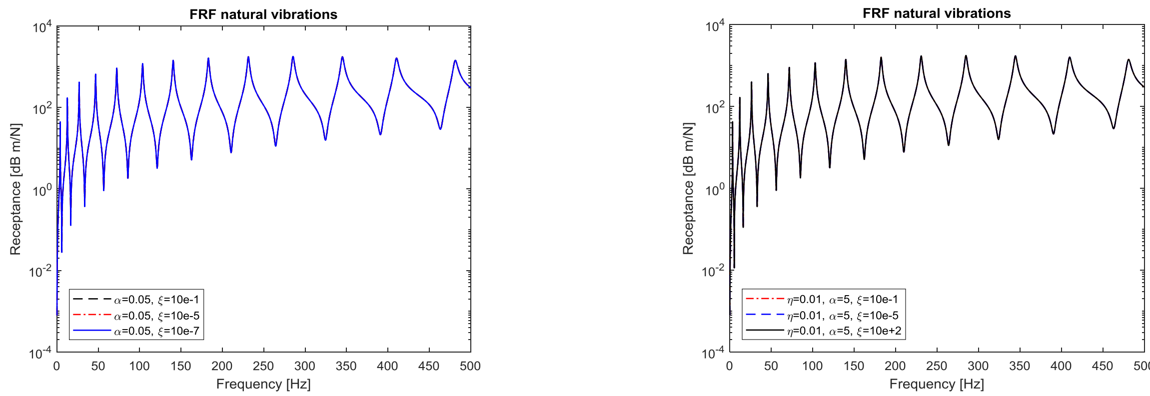

(c) (d)

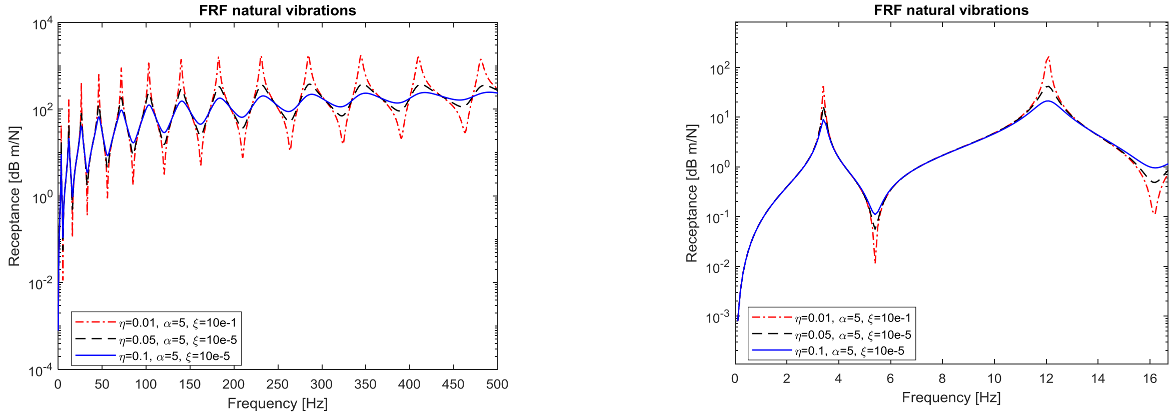

(e) (f)

Fig. 9 FRF functions for the natural vibration of the conductor, aerodynamic damping, T=0.1 kN, (a), (b) for different value of aerodynamic damping α and fixed values of material damping ratio ξ, (c), (d) for different value of material damping ratio ξ and fixed values of aerodynamic damping α, (e), (f) for different value of hysteretic loss factor

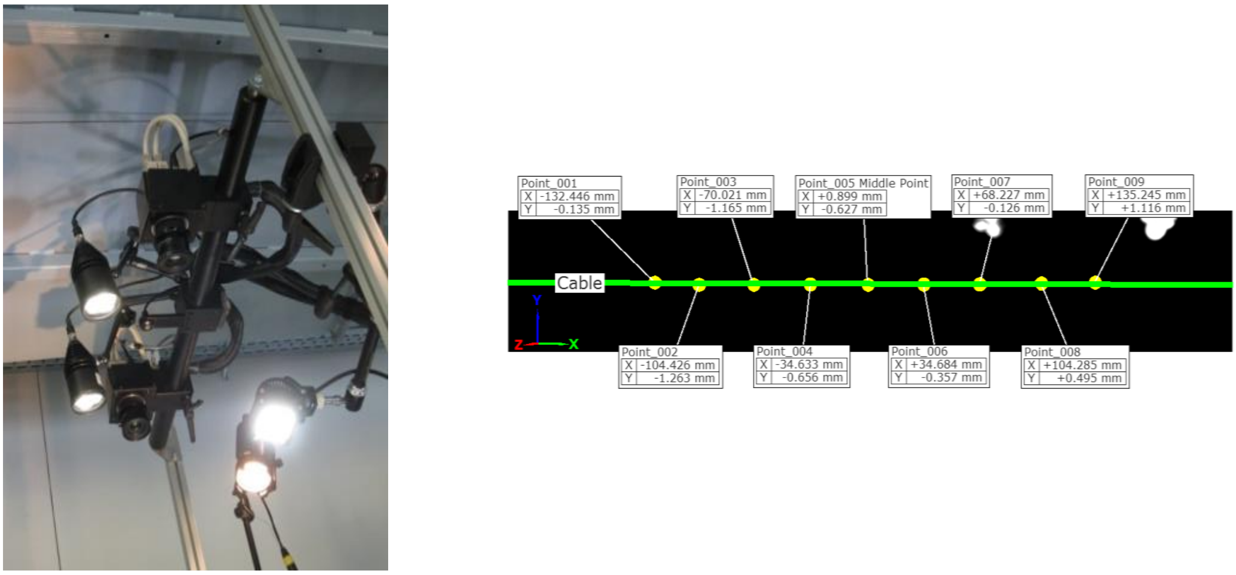

(a) (b)

Fig. 10 Measuring set-up, (a) camera recording system, (b) marking of measuring points

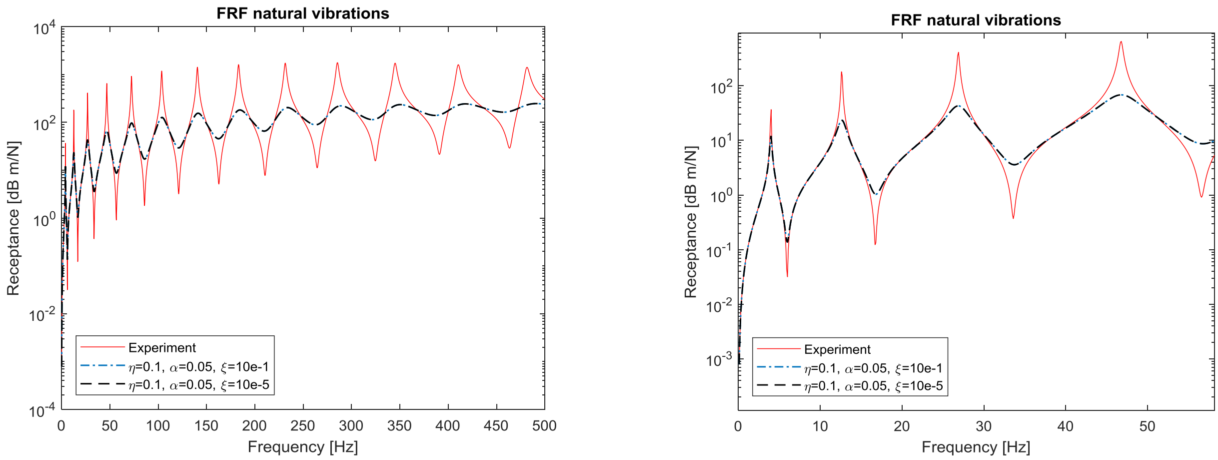

(a) (b)

Fig. 11 Comparison of FRF functions for the natural vibrations, tension T=0.1 kN, obtained in experiment and in numerical simulations of the conductor for different value of material damping ratio ξ

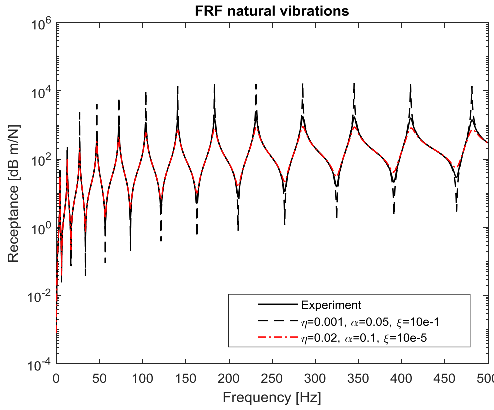

(a)

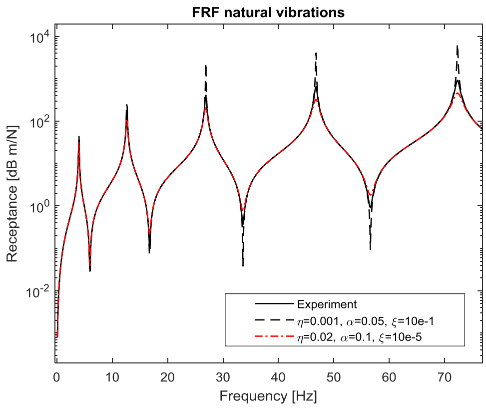

(b) Zoom

Fig. 12 Comparison of FRF functions for the natural vibrations, tension T=0.1 kN, obtained in experiment and in numerical simulations of the conductor for different value of hysteretic loss factor η, aerodynamic damping α and material damping ratio ξ. Best fit function achieved for η=0.02, α=0.1, ξ=10e-5

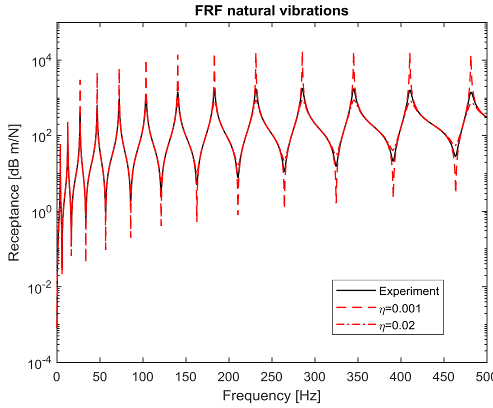

(a)

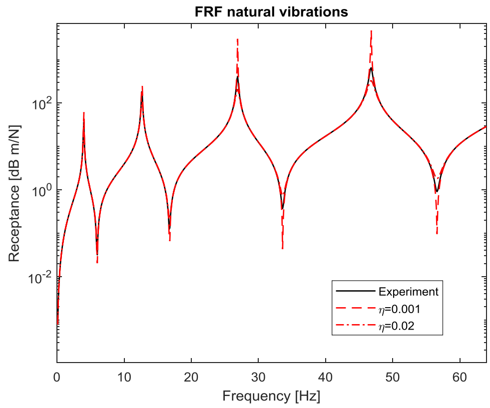

(b) Zoom

Fig. 13 Comparison of FRF functions for the natural vibrations, tension T=0.1 kN, obtained in experiment and in numerical simulations in the case of hysteretic damping only, for different value of hysteretic loss factor η

5. Experiments and results

The purpose of the experiments was to analyze the natural vibrations caused by the unit impulse force. Natural vibrations were investigated in the test section of dimensions 500 x 700 -2000mm. The flexible conductor model had a parameters as described in the section 4 of this paper. The conducting part was covered with a flexible rubber skin. The conductor was axially tensioned with a tension of 0.1 kN. For the purpose of vibration measurement the Digital Image Correlation (DIC) method was applied with use of CCD (Charge Couple Device) camera of the GOM Pontos 12M system (Fig.10a). In this case the dots with reflected layer were put on the conductor (Fig.10b). Dimensions of markers were 2mm and calculated using the geometrical features of DIC system and test details of dimensions of measurements. Testing procedure was designed to check the correctness of PONTOS 12M for detection of acceleration components in 3D measurements. The measurement system included two cameras, working stations and calibration equipment. The CCD camera worked at the resolution of 4096x3072 pixels and the sampling rate was equal to 256 Hz.

Figs.11-13 show the comparison of FRF functions for the natural vibration obtained in experiment and in

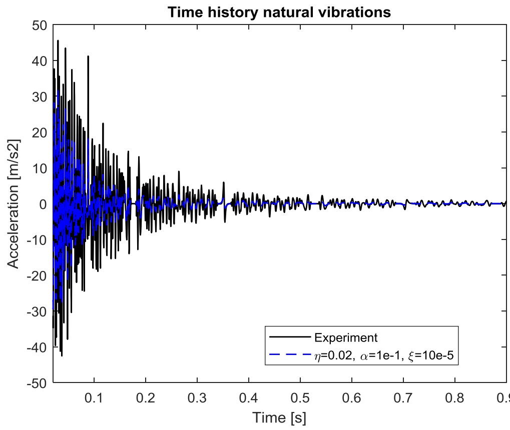

Fig. 14 Time history natural vibrations obtained in the experiment and in the simulation for the parameter of damping: L_1=0.035, η=0.02, α=0.1, ξ=10e-5

numerical simulations of the conductor for different value of hysteretic loss factor η and with aerodynamic damping (Fig.11), for parameters of best fit function: η=0.02, α=0.1, ξ=10e-5 (Fig.12) and for different value of hysteretic loss factor η (Fig. 13).

Fig. 14 presents the time history natural vibrations obtained in the experiment and in the simulation for the parameter of damping: η=0.02, α=0.1, ξ=10e-5.

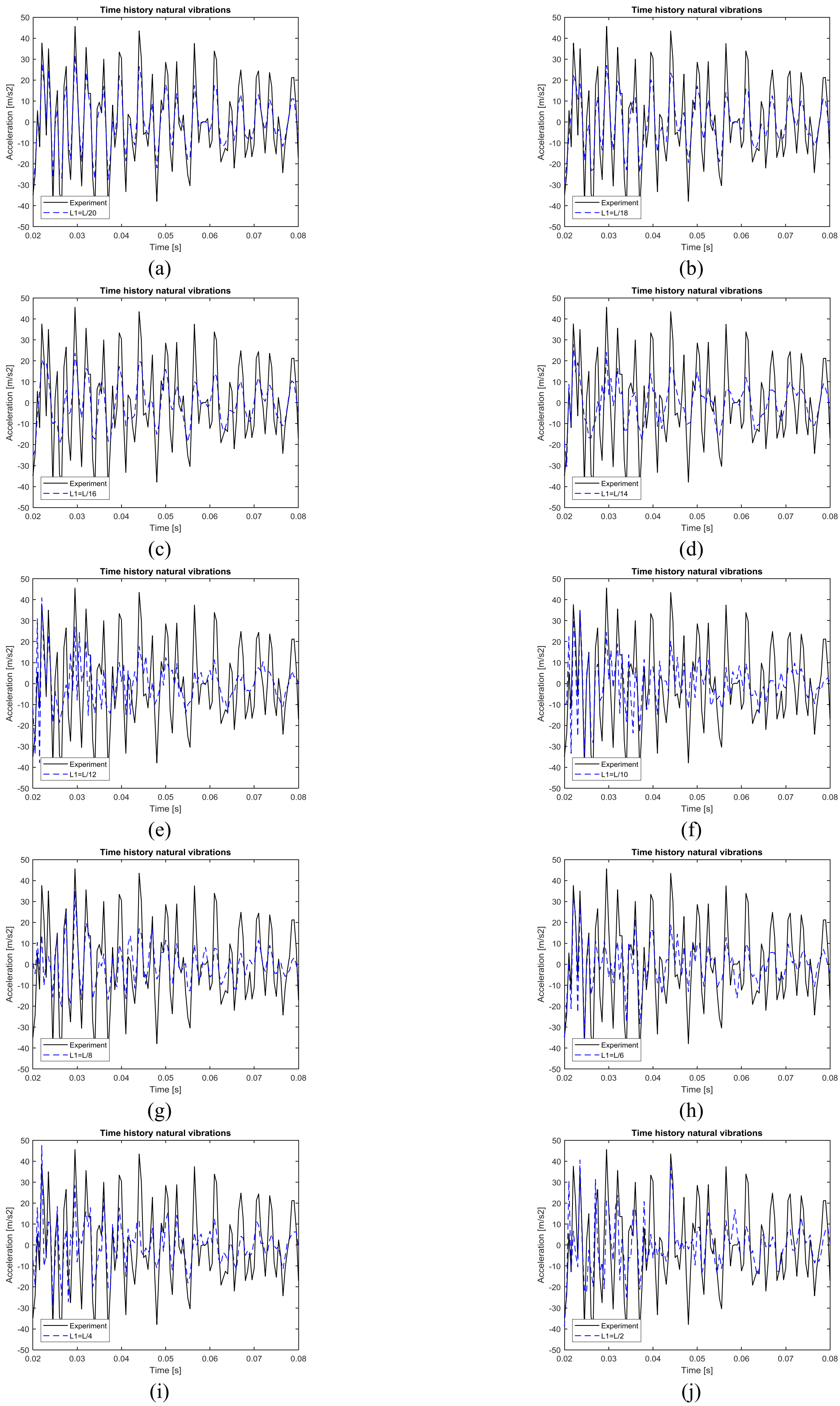

Fig. 15 Zoom of time history natural vibrations obtained in the experiment and in the simulation for the parameter of damping η=0.02, α=0.1, ξ=10e-5 and for different length of spectral element (a)-(j)

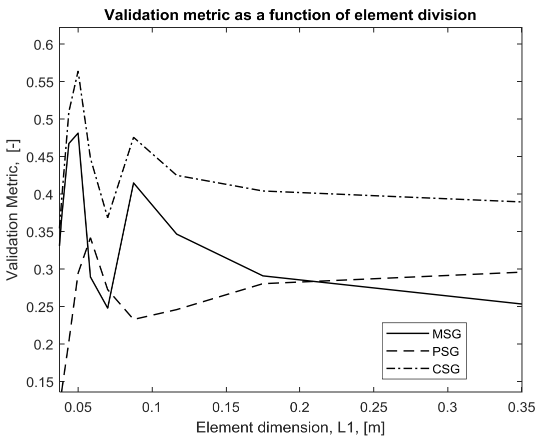

Fig. 16 Validation metrics for experimental and simulation results for different spectral element length, damping parameters η=0.02, α=0.1, ξ=10e-5

Table 2 Validation metrics for experimental and simulation results for different spectral element length, damping parameters η=0.02, α=0.1, ξ=10e-5.

L_1 , [m]	Natural vibrations		
	M_{SG}	P	C_{SG}
0.035	0,269216	0,109515	0,290639
0.039	0,368617	0,137097	0,393286
0.0875	0,414985	0,232857	0,475852

Fig. 15 presents the time history natural vibrations obtained in the experiment and in the simulation for the parameter of damping η=0.02, α=0.1, ξ=10e-5 and for different length of spectral element.

Fig. 15 Zoom of time history natural vibrations obtained in the experiment and in the simulation for the parameter of damping η=0.02, α=0.1, ξ=10e-5 and for different length of spectral element (a)-(j)

The results of validation metric analysis are shown in Fig.16 and in Table 2. As the validation process consisted in determining the validation coefficients and checking whether these coefficients are smaller than the assumed level of 30%, this criterion was fulfilled by simulation parameters of L_1=0.035, η=0.02, α=0.1, ξ=10e-5.

6. Conclusions

In the paper the analysis of natural vibrations of the transmission line with use of spectral elements and the laboratory experiments was performed. Investigations were carried out on transmission line with the span of 0.7 m. Particular attention was paid to the hysteretic and aerodynamical damping analysis. Sensitivity of the wave number was performed for changing of the tension force and damping parameters.

The numerical model was made using the Spectral Element Method. Experimental data from measurements was used in the estimation process, frequency response functions and time history dependences were compared for experiment and simulation results. In the spectral model, for various parameters of damping and tension force, the system response was checked and compared to the results of the vibration accelerations obtained in the measurement. The frequency analysis was carried out. The credibility of the model was assessed through a validation process carried out by comparing graphical plots of FRF functions and numerical values expressing differences in acceleration amplitude, phase angle differences and differences in acceleration and phase angle total values. The validation process consisted in determining the validation coefficients and checking whether these coefficients are smaller than the assumed level of 30%.

The next aspect constituting the purpose of this article was to present the wide possibilities of modelling and simulation of slender conductors using the Spectral Element Method. The obtained results show very good accuracy in the range of both experimental measurements as well as simulations analysis. The paper emphasizes the ease with which the sensitivity of the cable and its response to changes in density of spectral mesh division, tensile force or damping parameters can be studied.

In the paper, a very important issue of vibration of the actual transmission line was performed. In the literature, there are not too many studies on modern constructions of high-voltage transmission lines under real working conditions. It is worth noting that the presented results bring closer the producers and users of power transmission lines for the application of more durable cables than those currently used and more resistant to fatigue damage being the main cause of cable breakages and transmission infrastructure.

References

Aeschliman, D.P., Oberkampf, W.L. and Blottner, F.G. (1995), "A proposed methodology for CFD code verification, calibration, and validation", 95-CH3482-7; *16th International Congress on Instrumentation for Aerospace Simulation Facilities*, Dayton, OH, USA.

Aeschliman, D.P. and Oberkampf, W.L. (1998), "Experimental methodology for computational fluid dynamics code validation", *AIAA J.*, **36**(5), 733-741. https://doi.org/10.2514/2.461.

American Institute of Aeronautics and Astronautics (AIAA) (1998), "Guide for the verification and validation of computational fluid dynamics simulations", AIAA-G-077-1998; American Institute of Aeronautics and Astronautics, Reston, VA, USA.

American Society of Mechanical Engineers (ASME) (2006), "Guide for the verification and validation in computational solid mechanics", ASME VV 10-2006, ASME; New York, NY, USA.

Barber, T.J. (1998), "Role of code validation and certification in the design environment", *AIAA J.*, **36**(5), 752-758. https://doi.org/10.2514/2.433.

Benek, J.A., Kraft, E.M. and Lauer, R.F. (1998), "Validation issues for engine – Airframe integration", *AIAA J.*, **36**(5), 759-764. https://doi.org/10.2514/2.434.

Bertin, J.J., Martellucci, A., Neumann, R.D. and Stetson, K.F. (1993), "Developing a data Bbase 94 for the calibration and validation of hypersonic CFD codes - Sharp cones", *the 24th AIAA Fluid Dynamics Conference*, Orlando, FL, USA, July. https://doi.org/10.2514/6.1993-3044.

Boseop, J., Taehyun, K. and Usik, L. (2018), "Vibration analysis of a multi-span beam subjected to a moving point force using spectral element method", *Struct. Eng. Mech.*, **65**(3), 263-274.

https://doi.org/10.12989/sem.2018.65.3.263.

Bradley, R.G. (1988), "CFD validation philosophy, AGARD-CP-437", *Fluid Dynamics Panel Symposium: Validation of Computational Fluid Dynamics*, Lisbon, Portugal, May.

Clough, R. and Penzien, J. (1993), *Dynamics of Structures*, McGraw Hill, New York, USA.

Coleman, H.W. and Stern, F. (1997), "Uncertainties and CFD code validation", *J. Fluids Eng.*, **119**, 795-803. https://doi.org/10.1115/1.2819500.

Den Hartog, J.P. (1932), "Transmission line vibration due to sleet", *Transactions of the American Institute of Electrical Engineers*, **51**(4), 1074-1086. https://doi.org/10.1109/T-AIEE.1932.5056223.

Doyle, J.F. (1997), *Wave Propagation in Structures: Spectral Analysis Using Fast Discrete Fourier Transforms*, 2nd Edition, Springer-Verlag, New York, USA.

Dutkiewicz, M. (2017a), "Experimental measurements of dynamical wind load acting on the overhead transmission line", *Anul XXIV*, **1**, 88-100.

Dutkiewicz, M. (2017b), "Interaction of bridge cables and wake behind in the vortex induced vibrations", *14th International Conference Dynamical Systems - Theory and Application*s, Łódź, Poland, December.

Dutkiewicz, M., Machado, M.R. (2019a), "Spectral approach in vibrations of overhead transmission lines", *IOP Conference Series: Materials Science and Engineering 471*. https://doi.org/10.1088/1757-899X/471/5/052029.

Dutkiewicz, M. and Machado, M.R. (2019b), "Dynamical response of overhead transmission line in turbulent wind flow with application of the spectral element method", *IOP Conference Series: Materials Science and Engineering 471*. https://doi.org/10.1088/1757-899X/471/5/052031.

Fabro, A.T., Ritto, T.G., Sampaio, R. and Arruda, J.R.F. (2010), "Stochastic analysis of acracked rod modeled via the spectral element method", *Mech. Res. Communications*, **37**, 326-331.

Flynn, E.B., Todd, M., Croxford, J., Drinkwater, B. and Wilcox, P. (2011), "Enhanced detection through low order stochastic modeling for guided-wave structural health monitoring", *Struct. Health Monitoring*, **1**, 1-12. https://doi.org/10.1177/1475921711414232.

Geers, T.L. (1984), "An objective error measure for the comparison of calculated and measured transient response histories", *Shock Vib. Bull.*, **54**, 99-107.

Gołębiowska, I., Dutkiewicz, M. and Usewicz, B. (2015), "Methods of damping of overhead transmission lines", TTS, **12**(5), 2544-2548.

Gołębiowska, I. and Dutkiewicz, M. (2016), "The effectiveness of vibration damper attached to the cable due to wind action", *Intern. Conf. Exper. Fluid Mech.*, 209-213, Czech Republic, October.

Gołębiowska, I. and Dutkiewicz, M. (2017a), "Vortex induced vibration and wind flow around bridge cables", *Proceedings of 14th International Conference on Acoustics and Vibration of Mechanical Structures*, Timisoara, Romania, May.

Gołębiowska I. and Dutkiewicz M. (2017b), "Analysis of wind flow around the bridge cable", *Proceedings of 2th International Symposium on World Multidisciplinary Civil Engineering, Architecture and Urban Planning*, Prague, Czech Republic, June.

Gołębiowska I. and Dutkiewicz M. (2018), "Galloping of overhead power lines conductors", *Proceedings of 24th International Conference on Engineering Mechanics*, 257-260, Svratka, Czech Republic, May.

Gopalakrishnan, S., Chakraborty, A. and Mahapatra, D.R. (2007), *Spectral Finite Element Method*, Springer Verlag, New York, USA.

Machado, M.R. and Santos, J. (2015), "Reliability analysis of damaged beam spectral element with parameter uncertainties", *Shock Vib.*, **2015**. http://dx.doi.org/10.1155/2015/574846.

Machado, M., Adhikari, S. and Santos, J. (2017), "A spectral approach for damage quantifcation in stochastic dynamic systems", *Mech. Syst. Signal Proc.*, **88,** 253-278.

Lee, M., Park, I. and Lee, U. (2017), "An approximate spectral element model for the dynamic analysis of an FGM bar in axial vibration", *Struct. Eng. Mech.*, **61**(4), 551-561.

Lee, U. (2004), *Spectral Element Method in Structural Dynamics*, Inha University Press, Inha Univerity Incheon, Korea.

Lee, U. (2009), *Spectral Element Method in Structural Dynamics*, Wiley and Sons, Singapore.

Luongo, A., Zulli, D. and Piccardo, G. (2009), "On the effect of twist angle on nonlinear galloping of suspended cables", *Comput. Struct.*, **87**(15-16), 1003-1014.

Matt, C.F. and Castello, D.A. (2007), "On the numerical identification of the bending stiffness and the damping of transmission line conductors", *Proceedings of the XII International Symposium on Dynamic Problems of Mechanics*, Ilha Bela, Sao Paulo, Brazil, March.

Mehta, U.B. (1996), "Guide to credible computer simulations of fluid flows", *J. Propulsion Power*, **12**(5), 940-948. https://doi.org/10.2514/3.24126.

Meynen, H., Verma, P., Hagedorn, P. and Schafer, M. (2005), "On the numerical simulation of vortex-induced vibrations of oscillating conductors", *J. Fluids Struct.*, **21**(1), https://doi.org/10.1016/j.jfluidstructs.2005.05.019.

Oberkampf, W.L and Trucano, T.G. (2002), "Verification and validation incomputational fluid dynamics", *Prog. Aerosp. Sci.,* **8**, 209-272.

Rao, S.S. (2008), *Mechanical Vibration,* Pearson Prentice Hall, New Jersey, USA.

Russell, D.M. (1997), "Error measures for comparing transient data: part I: development of a comprehensive error measure", *Proceedings of the 68th Shock and Vibration Symposium*, 175-184. Hunt Valley, Maryland, November.

Schwer, L.E. (2007), "Validation metrics for response histories: Perspectives and case studies", *Eng. Comput.*, **23**, 295-309.

Sprague, M.A. and Geers, T.L. (2003), "Spectral elements and field separation for an acoustic fluid subject to cavitation", *J. Comput. Phys.* **184**, 149-162. https://doi.org/10.1007/s00366-007-0070-1.

Vecchiarelli, J., Curie, I.G. and Havard, D.G. (2000), "Computational analysis of aeolian conductor vibration with a stockbridge-type damper", *J. Fluids Struct.*, **14**, 489-509. https://doi.org/10.1006/jfls.1999.0279.

Wang, H.Q., Miao, J.C., Luo, J.H., Huang, F. and Wang, L.G. (1997), "The free vibration of long-span transmission line conductors with dampers", *J. Sound Vibr.*, **208**(4), 501.

William, L., Oberkampf, W.L. and Barone, M.F. (2006), "Measures of agreement between computation and experiment: Validation metrics", *J. Comput. Phys.,* **217**, 5-36. https://doi.org/10.1016/j.jcp.2006.03.037.

William, L. Oberkampf, W.L. and Smith, B. (2014), "Assessment criteria for computational fluid dynamics validation benchmark experiments", *52nd Aerospace Sciences Meeting*, AIAA SciTech Forum, (AIAA 2014-0205), https://doi.org/10.2514/6.2014-0005.

Yu, B.Y.J. and Soliman, M. (2014), "Estimation of cable tension force independent of complex boundary conditions", *ASCE J. Eng. Mech.*, **60**, 1-8. https://doi.org/10.1061/(ASCE)EM.1943-7889.0000836.

Zienkiewicz, O.C. and Taylor R.L. (1991), *The Finite Element Method*, 4th Edition, McGraw-Hill, London, United Kingdom.

CC